



## Measurement of $Z/\gamma^* \rightarrow \mu^+\mu^- + \text{jets}$ Production Cross Section

The CDF Collaboration  
URL <http://www-cdf.fnal.gov>  
(Dated: July 10, 2010)

Preliminary results on inclusive  $Z/\gamma^*$  boson plus jets production in  $p\bar{p}$  collisions at  $\sqrt{s} = 1.96$  TeV are presented. The measurement is based on  $6.0 \text{ fb}^{-1}$  of data collected with the CDF detector in run II. Inclusive jet cross sections are measured as a function of  $p_T^{jet}$  and jet multiplicity for jets in the region  $p_T^{jet} \geq 30 \text{ GeV}/c$  and  $|y^{jet}| \leq 2.1$ , in events in which the  $Z/\gamma^*$  boson decays into a muon pair. Results are compared to next-to-leading order perturbative QCD predictions.

## I. INTRODUCTION

The measurement of the inclusive production of collimated jets of hadrons in association with a  $Z/\gamma^*$  boson in  $p\bar{p}$  collisions provides a stringent test of perturbative QCD [1]. The  $Z/\gamma^* + \text{jets}$  final state is also one of the main backgrounds in searches for new physics like, for example, the Higgs boson in the  $Z + H$  channel, and supersymmetry in the  $\cancel{E}_T + \text{jets}$  channel. We report on preliminary measurements of  $Z/\gamma^* \rightarrow \mu^+\mu^- + \text{jets}$  production using  $6.0 \text{ fb}^{-1}$  of data collected with the CDF detector in run II. The CDF detector is described in detail elsewhere [2]. This measurement follows previous studies on  $Z/\gamma^* \rightarrow e^+e^- + \text{jets}$  at CDF [3]. The measured cross sections are corrected back to particle level and compared to next-to-leading order (NLO) pQCD predictions including non-perturbative contributions. Inclusive jet differential cross section as a function of  $p_T^{jet}$  [17] in events with at least one and two jets in the final state, and the total cross section as a function of inclusive jet multiplicity are measured [18].

## II. MONTE CARLO SIMULATION

Monte Carlo simulated samples are used to model the  $Z/\gamma^* \rightarrow \mu^+\mu^- + \text{jets}$  signal reconstruction, estimate background contributions, unfold the measurements back to the particle level, and evaluate non-pQCD corrections applied to the NLO predictions. ALPGEN v2.10' interfaced to PYTHIA v6.325 [4] is used as event generator, with CTEQ5L parton distribution function (PDF) for the colliding proton and antiproton [5]. Tune BW parameters are employed to govern the underlying event. A full CDF detector simulation based on GEANT3 [8] is applied to the generated samples and the GFLASH [9] package is used to simulate the energy deposition in the calorimeter.

## III. EVENT SELECTION

Events are collected using a high  $p_T$  muon trigger, whose minimum  $p_T$  threshold is  $18 \text{ GeV}/c$ . Events are required to have a reconstructed primary vertex with  $z$  position within  $60 \text{ cm}$  from the nominal interaction point. Muons are identified offline on the basis of tracking and calorimeter information. The impact parameter of the track has to be consistent with the particle originating from the primary interaction vertex and the energy deposition in the calorimeter is required to be consistent with those expected from a minimum-ionizing particle. Further cuts on the number of hits in the tracking system,  $\chi^2$  and residuals of the track fit are applied to reduce the background of kaons and pions which have decayed in flight. A  $Z/\gamma^* \rightarrow \mu^+\mu^-$  boson is identified requiring two reconstructed muons with  $p_T > 25 \text{ GeV}/c$  and  $|\eta| < 1.0$ , associated to tracks which are opposite charged, and with invariant mass in the range  $66 \leq M_{\mu\mu} \leq 116 \text{ GeV}/c$ . Trigger and muon identification efficiencies are evaluated on data with a tag-leg versus probe-leg method.  $Z/\gamma^* \rightarrow \mu^+\mu^-$  events are selected requiring one muon leg to pass a set of tight identification cuts (tag-leg), and the other muon leg to meet kinematic requirements (probe-leg). The second leg is then used as a probe muon to evaluate the efficiencies of trigger and identification requirements. The resulting efficiencies are used to evaluate the  $Z/\gamma^* \rightarrow \mu^+\mu^-$  inclusive cross section, which is checked against the next-to-leading order prediction and the published CDF result [10].

## IV. JET RECONSTRUCTION

Jets are reconstructed in data and Monte Carlo simulated events from the energy deposits in the calorimeter towers with transverse momenta [19] above  $0.1 \text{ GeV}/c$ . Jets are searched for using the midpoint algorithm [11] with cone radius  $R = 0.7$  and a merging/splitting fraction of 0.75, starting from seed towers with transverse momenta above  $1 \text{ GeV}/c$ . The same algorithm is applied to the final state particles in the Monte Carlo generated events, excluding  $Z/\gamma^*$  decay products, to define jets at the particle level. The measured jet transverse momentum  $p_T^{jet}$  systematically underestimates that of the particle-level jet. For  $p_T^{jet}$  values about  $30 \text{ GeV}/c$ , the jet transverse momentum is underestimated by about 30%. The systematic shift decreases with increasing  $p_T^{jet}$  down to about 11% for  $p_T^{jet} > 200 \text{ GeV}/c$ . This is mainly attributed to the presence of inactive material and the non-compensating nature of the calorimeter [12]. An average correction, as a function of  $p_T^{jet}$  and  $y^{jet}$ , is applied to the measured  $p_T^{jet}$  to account for these effects [13]. The measured  $p_T^{jet}$  also includes contributions from multiple  $p\bar{p}$  interactions per crossing at high instantaneous luminosity. Multiple interactions are identified via the presence of additional primary vertices reconstructed from charged particles. For each jet,  $p_T^{jet}$  is corrected for this effect by removing a certain amount of

transverse momentum,  $\delta_{p_T}^{\text{mi}} = 1.06 \pm 0.32 \text{ GeV}/c$ , for each additional primary vertex in the event, as determined from data [13]. After these corrections, jets with  $p_T^{\text{jet}} \geq 30 \text{ GeV}/c$  and  $|y^{\text{jet}}| \leq 2.1$  are selected. A minimum distance between the jets and the muons ( $\Delta R_{\mu\text{-jet}} > 0.7$ ) is also required. The measured jet cross sections are corrected for acceptance and smearing effects back to the particle level using ALPGEN+PYTHIA-TUNE BW Monte Carlo event samples, and a bin-by-bin unfolding procedure that also accounts for the efficiency of the  $Z/\gamma^* \rightarrow \mu^+\mu^-$  selection criteria.

## V. BACKGROUNDS ESTIMATION

Background estimation is done both with Monte Carlo and data-driven techniques. The contribution coming from QCD dijet, W+jets and decayed in flight particles is estimated from data. Events are selected with the same criteria described in Section III, with the exception that the two muon tracks are required to be same charged. The same charge events yield is then directly considered as the background estimation for QCD, W+jets and decays-in-flight. Other contributions coming from electroweak processes and  $t\bar{t}$  events are computed using MC sample. Figure 1 shows the invariant mass distribution of reconstructed  $Z/\gamma^* \rightarrow \mu^+\mu^-$  in data compared to background plus Monte Carlo signal prediction, in events with  $\geq 1$  jet and  $\geq 2$  jets in the final state. The number of estimated background events and data event yields for  $\geq 1, 2$  and  $3$  jets are reported in table I.

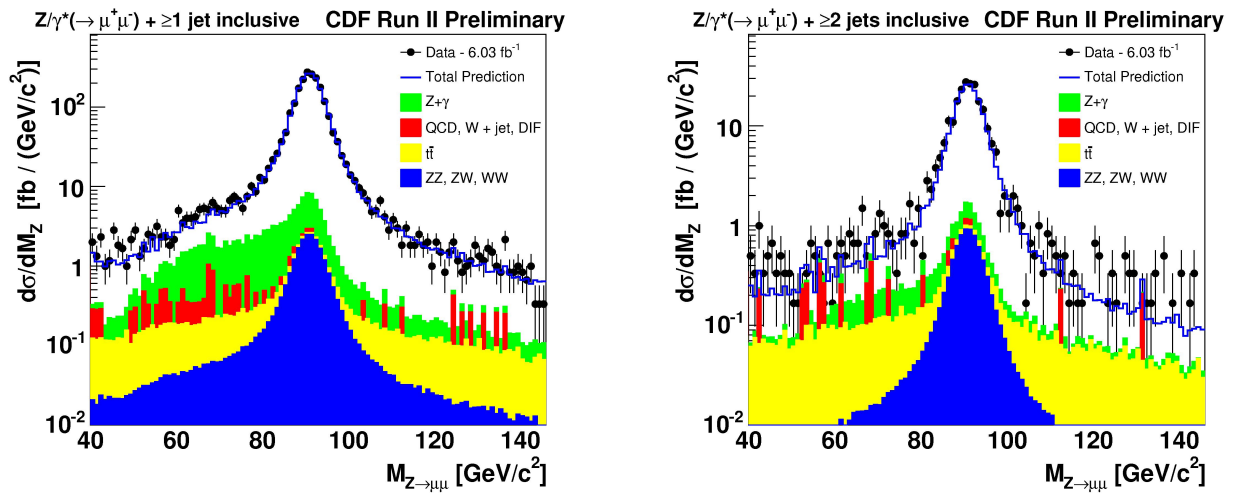


FIG. 1: Data and signal plus background estimation within Z mass window and on side bands, in (left)  $Z + \geq 1$  jet and (right)  $Z + \geq 2$  jets events.

CDF II Preliminary			
Backgrounds	Estimated events in $6.03 \text{ fb}^{-1}$		
	$Z + \geq 1 \text{ jet}$	$Z + \geq 2 \text{ jets}$	$Z + \geq 3 \text{ jets}$
$Z/\gamma^* \rightarrow \mu^+\mu^- + \gamma$	$495.5 \pm 148.6$	$39.9 \pm 12.0$	$2.4 \pm 0.7$
$WW, ZZ, ZW$	$134.3 \pm 40.3$	$48.9 \pm 14.7$	$4.9 \pm 1.5$
QCD, W+jets and DIF	$72 \pm 72$	$20 \pm 20$	$2.0 \pm 2.0$
$t\bar{t}$ production	$44.2 \pm 13.2$	$25.1 \pm 7.5$	$3.1 \pm 0.9$
$Z \rightarrow \tau^+\tau^- + \text{jets}$	$3.6 \pm 1.1$	$1.7 \pm 0.5$	$0.0 \pm 0.0$
<b>Total Backgrounds</b>	<b><math>750 \pm 171</math></b>	<b><math>136 \pm 29</math></b>	<b><math>12.3 \pm 2.7</math></b>
<b>Data</b>	<b><math>13247 \pm 115</math></b>	<b><math>1485 \pm 39</math></b>	<b><math>133.0 \pm 11.5</math></b>

TABLE I: Estimated background events in  $6.03 \text{ fb}^{-1}$  for  $Z/\gamma^* \rightarrow \mu^+\mu^- + \geq 1, 2$  and  $3$  jets compared to data yield.

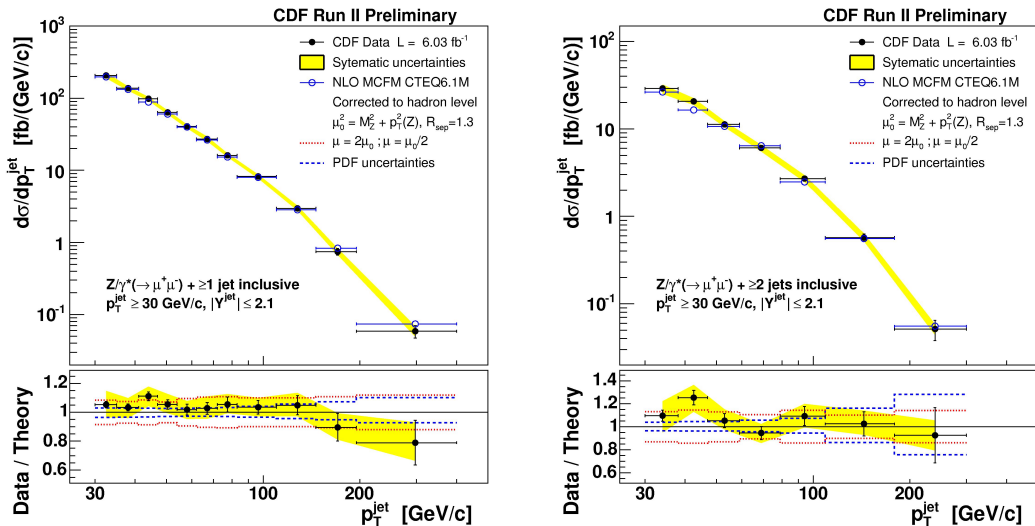


FIG. 2: Measured inclusive jet differential cross section as a function of  $p_T^{jet}$  (black dots) in  $Z/\gamma^* + \geq 1$  jet and  $Z/\gamma^* + \geq 2$  jets events compared to NLO pQCD predictions (open circles). The shaded bands show the total systematic uncertainty, except for the 5.8% luminosity uncertainty. The dashed and dotted lines indicate the PDF uncertainty and the variation with  $\mu_0$  of the NLO pQCD predictions, respectively.

## VI. SYSTEMATIC UNCERTAINTIES

Several sources of systematic uncertainty to the measured cross section have been considered. The uncertainties on trigger and muon ID efficiencies are evaluated assuming a binomial distribution and the propagated uncertainty on the cross sections is 0.2%. The jet energies are varied by 2% at low  $p_T^{jet}$  and up to 2.7% at high  $p_T^{jet}$  to account for the uncertainties on the absolute energy scale in the calorimeter [13]; this introduces uncertainties on the final measurements which vary between 5% at low  $p_T^{jet}$  and 12% at high  $p_T^{jet}$ . The  $y^{jet}$  dependence of the average correction applied to  $p_T^{jet}$  introduces a 2% uncertainty on the measured cross sections, approximately independent of  $p_T^{jet}$ . The uncertainty on  $\delta_{p_T}^{mi}$  translates into uncertainties between 1% and 8% on the measured cross sections. A conservative 100% uncertainty is assigned to the QCD, W+jets and decay-in-flight background contribution, which translates into uncertainties between 1% and 5% in the final results. A 30% uncertainty is assigned to the rest of the background contributions, which are evaluated with Monte Carlo simulation, leading to uncertainties between 1% and 3% on the measured cross sections. Positive and negative deviations with respect to the measured cross section values are added separately in quadrature to define the total systematic uncertainty. Finally the measurement is affected by an overall 5.8% uncertainty on the quoted total integrated luminosity.

## VII. NEXT-TO-LEADING ORDER PREDICTION

The NLO prediction are computed using the MCFM program [14]. The CTEQ6.1M PDFs[15] are employed and the renormalization and factorization scales are set to  $\mu_0^2 = M_Z^2 + p_T^2(Z)$ . Variation of the renormalization and factorization scales by a factor of two and half induces a change between 10% and 15% in the theoretical predictions. The uncertainty on the PDF is calculated with the Hessian method [16] and the corresponding uncertainties on the predictions vary from 2% at low  $p_T^{jet}$  to 15% at high  $p_T^{jet}$ . The theoretical predictions include parton-to-particle level correction factors that account for underlying event and fragmentation processes. These non-perturbative effects are estimated with PYTHIA-TUNE A Monte Carlo simulation. The correction is obtained evaluating the ratio of the  $p_T^{jet}$  and  $N_{jet}$  distributions between particle-level jets and parton-level jets reconstructed turning off both the interaction between proton and antiproton remnants and the string fragmentation in the Monte Carlo samples.

### VIII. RESULTS

Figure 2 shows the measured inclusive differential cross section in  $Z/\gamma^* + \geq 1$  jet and  $Z/\gamma^* + \geq 2$  jets events, for jets with  $p_T^{\text{jet}} \geq 30 \text{ GeV}/c$  and  $|y^{\text{jet}}| \leq 2.1$ . The measurements are well described by the NLO pQCD predictions. Figure 3 presents the measured cross section as a function of inclusive  $Z + \geq N_{\text{jet}}$  multiplicity compared to the NLO predictions. For  $N_{\text{jet}} \geq 3$  only LO predictions are available. Data are followed by the NLO predictions. The measurement suggests a common LO-to-NLO k-factor approximately independent of  $N_{\text{jet}}$ .

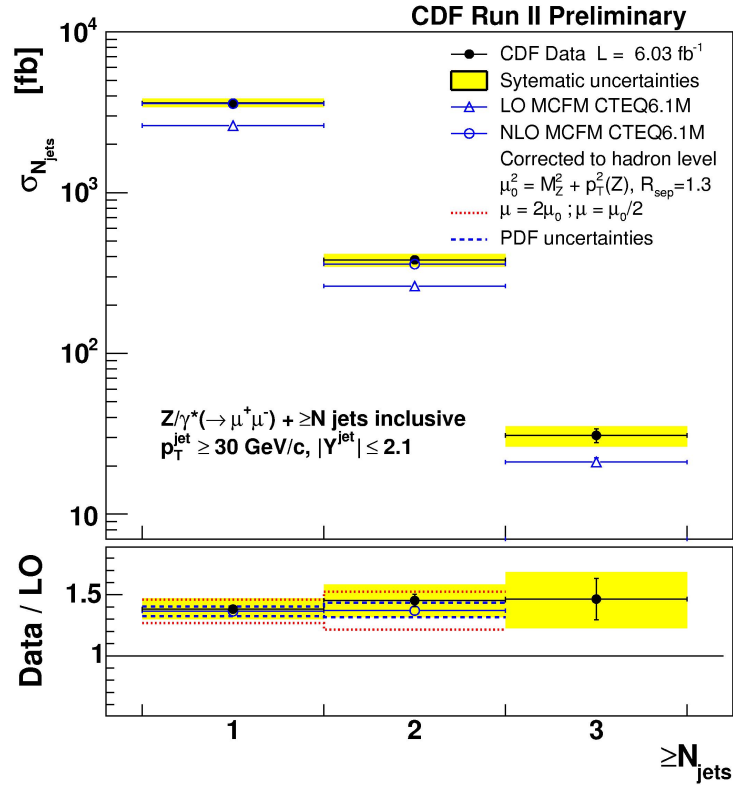


FIG. 3: (top) Measured total cross section for inclusive jet production in  $Z/\gamma^* \rightarrow \mu^+\mu^-$  events as a function of  $N_{\text{jet}}$  compared to LO and NLO pQCD predictions. The shaded bands show the total systematic uncertainty, except for the 5.8% luminosity uncertainty. (bottom) Ratio of data and NLO to LO pQCD predictions versus  $N_{\text{jet}}$ . The dashed and dotted lines indicate the PDF uncertainty and the variation with  $\mu_0$  of the NLO pQCD predictions, respectively.

### Acknowledgments

We thank the Fermilab staff and the technical staffs of the participating institutions for their vital contributions. This work was supported by the U.S. Department of Energy and National Science Foundation; the Italian Istituto Nazionale di Fisica Nucleare; the Ministry of Education, Culture, Sports, Science and Technology of Japan; the Natural Sciences and Engineering Research Council of Canada; the National Science Council of the Republic of China; the Swiss National Science Foundation; the A.P. Sloan Foundation; the Bundesministerium für Bildung und Forschung, Germany; the World Class University Program, the National Research Foundation of Korea; the Science and Technology Facilities Council and the Royal Society, UK; the Institut National de Physique Nucleaire et Physique des Particules/CNRS; the Russian Foundation for Basic Research; the Ministerio de Ciencia e Innovación, and Programa

Consolider-Ingenio 2010, Spain; the Slovak R&D Agency; and the Academy of Finland.

---

- [1] D.J. Gross and F. Wilczek, Phys. Rev. D 836331973
- [2] F. Abe, et al., Nucl. Instrum. Methods Phys. Res. A **271**, 387 (1988); D. Amidei, et al., Nucl. Instrum. Methods Phys. Res. A **350**, 73 (1994); F. Abe, et al., Phys. Rev. D **52**, 4784 (1995); P. Azzi, et al., Nucl. Instrum. Methods Phys. Res. A **360**, 137 (1995); The CDFII Detector Technical Design Report, Fermilab-Pub-96/390-E
- [3] The CDF Collaboration Phys. Rev. Lett. **100** 102001 (2008).
- [4] T. Sjostrand et al., High-Energy-Physics Event Generation with PYTHIA 6.1, Comput. Phys. Commun. **135**, 238 (2001).
- [5] H.L. Lai *et al.*, Eur. Phys. J. C **12**, 375 (2000).
- [6] T. Affolder *et al.* (CDF Collaboration), Phys. Rev. D **65**, 092002 (2002)
- [7] O. Saltó, Ph.D. Thesis, U.A.B., Barcelona (2008).
- [8] R. Brun *et al.* Tech. Rep. CERN-DD/EE/84-1, 1987.
- [9] G. Grindhammer, M. Rudowicz, and S. Peters, Nucl. Instrum. Methods A **290**, 469 (1990).
- [10] D. Acosta *et al.* (CDF Collaboration), Phys. Rev. Lett. **94**, 091803 (2005).
- [11] A. Abulencia *et al.* (CDF Collaboration), Phys. Rev. D **74**, 071103(R) (2006).
- [12] S.R. Hahn *et al.*, Nucl. Instrum. Methods A **267**, 351 (1988).
- [13] A. Bhatti *et al.*, Nucl. Instrum. Methods A **566**, 375 (2006).
- [14] J. Campbell and R.K. Ellis, Phys. Rev. D **65** 113007 (2002).
- [15] J. Pumplin, *et al.*, JHEP **0207** 012 (2002).
- [16] J. Pumplin, *et al.*, Phys. Rev. D **65** 014013 (2001).
- [17] Coordinates are referred to a cylindrical system with the  $z$  axis along the beam line, polar angle  $\theta$  and azimuthal angle  $\phi$ . Transverse energy and momentum are defined as  $E_T = E \sin\theta$  and  $p_T = p \sin\theta$ , pseudorapidity and rapidity as  $\eta = -\ln(\tan(\frac{\theta}{2}))$  and  $y = \frac{1}{2}\ln(\frac{E+p_z}{E-p_z})$ .
- [18] Results, including also cross sections as a function of  $y^{jet}$ , are reported in [http://www-cdf.fnal.gov/physics/new/qcd/Zjets\\_mumu2010](http://www-cdf.fnal.gov/physics/new/qcd/Zjets_mumu2010)
- [19] The momentum is computed using the energy and the position with respect to the primary interaction vertex.